CrossMark

ORIGINAL ARTICLE

Structural–geological and karst feature investigations of the limestone–flysch thrust-fault contact using low-frequency ground penetrating radar (Adria–Dinarides thrust zone, SW Slovenia)

Marjana Zajc · Bogomir Celarc · Andrej Gosar

Abstract The Karstic thrust edge, a pronounced geomorphologic step, which is a result of the tectonostratigraphic evolution of the active Adria–Dinarides thrust zone, represents a major obstacle for the planned new railway route Divača–Koper. Thus, the geotechnical and structural properties as well as the geometry of the thrust-fault planes in this area are of great importance. Since geological mapping cannot give insight into the subsurface to reveal a complex 3D structure, and the numerous boreholes needed to investigate the area would be too expensive and time consuming, the application of a geophysical method such as ground penetrating radar (GPR) is needed. To test the method for determining near surface features and detecting low-angle inclined thrusts, a low frequency GPR system with 50 MHz rough terrain antenna was used to record 13 GPR profiles along all three floors of the Črnotiče quarry, where the spatial position of the Socerb thrust fault that separates limestones above and flysch layers below is relatively well documented. The profiles were positioned across selected existing boreholes. The GPR results were correlated with borehole data as well as geological mapping results. The GPR provided not only precise information on the geometry of the Socerb thrust

fault, but was also very useful for establishing the position of some known as well as several potential cavities, both air- and sediment-filled. In areas further from the thrust-fault zone, where the limestone is less tectonically damaged, it was also possible to determine apparent dip angles of the strata, which after reconstruction matched the true dips gathered from geological mapping.

Introduction

The thrust contact between the Adria Microplate and the Dinarides in the SW Slovenia consists of several superimposed thrust faults with different displacements (Placer et al. 2004; Vrabec and Fodor 2006; Placer et al. 2010; Fig. 1). Areas, where outcropping Eocene limestones are thrusted on the flysch sedimentary sequence along low-angle inclined thrust faults, form a prominent geomorphologic step named the Karstic edge (Placer 2002, 2005, 2007). This characteristic physiographic feature represents an obstacle for the planned new railway Divača–Koper (Celarc et al. 2012). Since the flysch is relatively more ductile in comparison to the more brittle limestones, it is usually highly tectonically deformed and sheared immediately below the thrust plane. Therefore, it is crucial to know its exact geotechnical and structural characteristics, its geometry and the extent of the thrust-fault plane(s), the structure of the footwall and hangingwall blocks, the development of possible karstic cavities in the limestones (e.g. Gosar 2012; Zajc et al. 2014) or contact karst type cavities at the flysch-limestone tectonic contacts (empty or

M. Zajc (✉) · A. Gosar
Faculty of Natural Sciences and Engineering, Department of Mining and Geotechnology, University of Ljubljana, Aškerčeva 12, 1000 Ljubljana, Slovenia
e-mail: marjana.zajc@ntf.uni-lj.si

B. Celarc
Geological Survey of Slovenia, Dimičeva 14, 1000 Ljubljana, Slovenia

A. Gosar
Slovenian Environment Agency, Seismology and Geology Office, Dunajska 47, 1000 Ljubljana, Slovenia

Springer

Fig. 1 **a** Geographical and
geotectonic (Vrabec and Fodor
2006) position of the research
area. **b** Adria–Dinarides thrust
zone and structural–geological
position of the Črnotiče quarry
[Placer et al. 2010 (modified)].
c Cross-section across the
research area
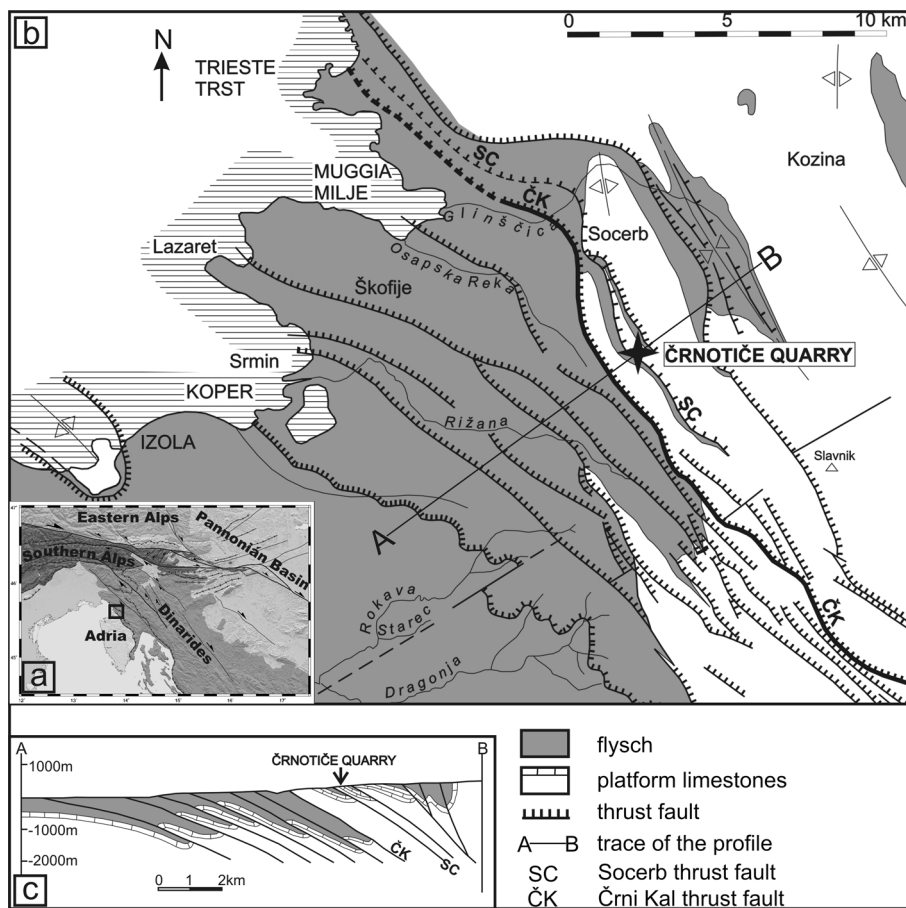
filled) and the level of the ground water table (Carriere
et al. 2013). Since the thrust-fault structures also cross a
few active limestone quarries in the area, the exploitation
companies need to know their geometry in detail to cal-
culate the quantities of the exploitable material in the
productive hangingwall, to plan excavations and to avoid
geological hazards for exploitation (Zajc et al. 2014).

To reveal structural characteristics and position of the
thrust-fault plane, the first, but not always the most precise
method, is geological mapping which is limited to the
surface. The structural characteristics of the subsurface
could be obtained with boreholes; however, this can be
relatively expensive, not to mention time consuming. For a
reliable determination of the complex 3D thrust-fault plane
geometry, numerous boreholes would be needed. With
oriented cores and televiewer well logging, the dip of the
thrust-fault plane in the borehole could be determined, but
it may represent only the local dip, which could be sig-
nificantly different from the dip in the quarry-size scale.
The application of various geophysical methods would thus
be a better option. To define the shallow-lying (up to 40 m
below the surface) thrust planes and the occurrence of
cavities, the use of the ground penetrating radar (GPR)

might be a good choice, especially where limestones,
which allow for good GPR penetration, are thrusted on the
flysch layers. The low-frequency GPR method has been
proven effective for determining near surface features
within carbonate rocks by many studies so far (e.g.
McMechan et al. 1998; Sigurdsson and Overgaard 1998;
Beres et al. 2001; Cunningham 2004; Pueyo-Anchuela
et al. 2009; Pavlič and Praznik 2011; dos Reis et al. 2014).

The main purpose of this investigation is to test the
application of the low-frequency GPR method for the
determination of the characteristics of the Socerb thrust
fault in the active Črnotiče limestone quarry (SW Slove-
nia), where limestones in the hangingwall block are thru-
sted on the flysch rocks in the footwall block along a low-
angle thrust plane. The structural characteristics of the
thrust-fault plane within the quarry are relatively well
defined with geological mapping, numerous boreholes and
continuous exploitation works. Profiles were positioned
across selected control boreholes. The relation between the
thrust-fault plane and the present surface (surface–fault
plane distance) allows us to study the area for a consider-
able distance along the dip of the tectonic plane and not
only along the strike.

Geological setting

Geology of the research area

The research area belongs to the Adria–Dinarides thrust zone, part of the External Dinaric Imbricate Belt (Placer et al. 2010; Fig. 1), which is tectonically still active (Vrabec and Fodor 2006; Rižnar et al. 2007; Weber et al. 2010). The tectonostratigraphic evolution of this area is the result of the carbonate sedimentation on the Adriatic–Dinaric Carbonate Platform from Late Triassic onwards, the degradation of the carbonate platform and the beginning of the clastic flysch deposition in front of the advancing Dinaric collision thrust system in the foreland flexure basin (Jurkovšek et al. 1996; Otoničar 2007; Korbar 2009). The Dinaric area and the Istria Peninsula area represent a tectonic contact between the Adria Microplate and the Dinarides (Handy et al. 2010), which started to form in Eocene (Vrabec and Fodor 2006). In Miocene, the Adria Microplate experienced segmentation and began rotating in the counter-clockwise direction and underthrusting beneath the Dinarides (Placer et al. 2010 and references there in). The result is the formation of the Adria–Dinarides thrust zone with NW–SW striking and SW foreland-verging thrust system, which consists of at least 11 recognised thrusts faults (Fig. 1), with each subsequent thrust fault being flatter in the foreland direction. Moderate secondary folding of thrust planes and poly-phase thrusting are common in this area (Placer et al. 2010). Depending on the cross-section of the thrust system with the present-day topography, there are three possibilities of the hangingwall–footwall block relations: (1) limestones are thrusted on limestones; (2) limestones are thrusted on flysch and (3) flysch is thrusted on flysch. For this study, the second situation is the most relevant as it is present in the wider area of the Črnotiče limestone quarry.

Geology and structure of the Črnotiče quarry

The active Črnotiče limestone quarry (Fig. 2a), size app. 600 × 600 m, with three exploitation floors at 387 m, 401–402 and 419 m a.s.l., with max. relative elevation difference of 58 m (Fig. 2b), is located in the Podgorski kras plateau (Mihevc 2007) and is structurally positioned in the Socerb thrust block, representing the hangingwall block of the Socerb thrust fault. The footwall block is named Črni Kal thrust block.

The lower part of both thrust blocks consists of the indistinctly medium-bedded Alveolinal–Nummulitic limestones (packstone–grainstone) of the Eocene (Ilerdian–Lutetian) age (Košir 2003; Jurkovšek 2008), deposited in the mid-ramp facies. Bedding planes are not represented by physical discontinuities, but rather by the interchanging of the darker–lighter tone of the individual beds. They pass upsection along a gradual transition into the marlstones, representing the lower part of the flysch sequence. The marlstones have a massive appearance, with no distinct bedding planes. The stratification is represented by lamination visible as darker or lighter bands in the fresh outcrops or borehole cores. The marlstones are tectonically deformed (sheared) along the contact with thrust-fault planes and primary structures are obliterated (unpublished data). The weathered (oxidised) zone in marlstone outcrops reaches 4–5 m below the surface. As discovered from boreholes, weathered marlstones also occur sporadically immediately below the thrust-fault plane and are related to karstic caverns appearing along the thrust contact between limestones and flysch layers. Karstic caverns and shafts, which are often filled with allochthonous sediments, autochthonous collapse material or cave sediments, are relatively frequent in the quarry (Mihevc 2000; Mihevc et al. 2002; Horaček et al. 2007).

The Socerb thrust fault outcrops immediately south of the quarry and is defined as a distinctive morphologic step connected with the NW–SE orientated hanging wall anticline in the Alveolinal–Nummulitic limestones forming the Socerb thrust–block. The anticline is clearly visible in the quarry, with its steeper SW and gentler NE limb and SW directed vergence. The thrust fault dips gently to the NE (50/15) as measured in the outcrops (Fig. 2). The thrust-fault plane and the footwall Črni Kal thrust block with outcropping flysch have been exposed during exploitation and can be seen in the quarry as a small tectonic window (Fig. 2c, d). Several exploration boreholes were drilled through the limestone, ending slightly below the thrust plane in the flysch unit of the footwall thrust block (unpublished data). Two of them penetrated the entire flysch unit and terminated in limestones that lie stratigraphically below the flysch (Celarc et al. 2012). Based on the data from the geological mapping and from the existing boreholes, the geometry (structure contours) of the thrust-fault plane was reconstructed (Fig. 2a). The thrust-fault plane dips to the NNE and is slightly folded, indicating several pulses of thrusting (Fig. 2d). Locally, a minor displacement along younger faults is visible, but has no significant influence on the overall picture. Immediately below the thrust-fault plane, marlstones are usually intensively deformed and sheared. In the quarry, tensional fractures are recognised in the limestones, striking in the NW–SE direction and dipping steeply to the NE in the SW limb of the anticline and to the SW in the NE limb of the anticline.

Methodology

The non-destructive nature and its great efficiency are the main reasons for the rapid increase of the use of the GPR
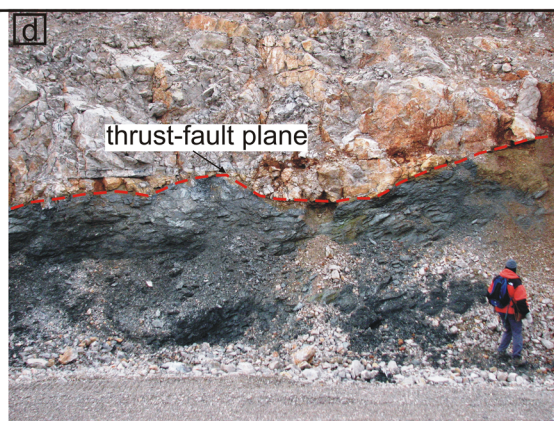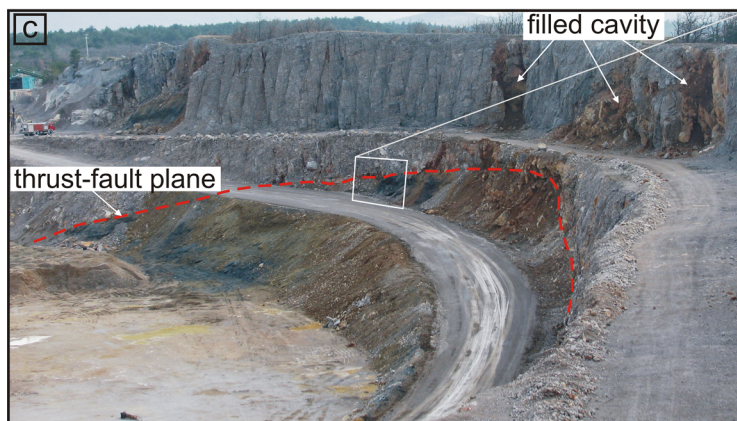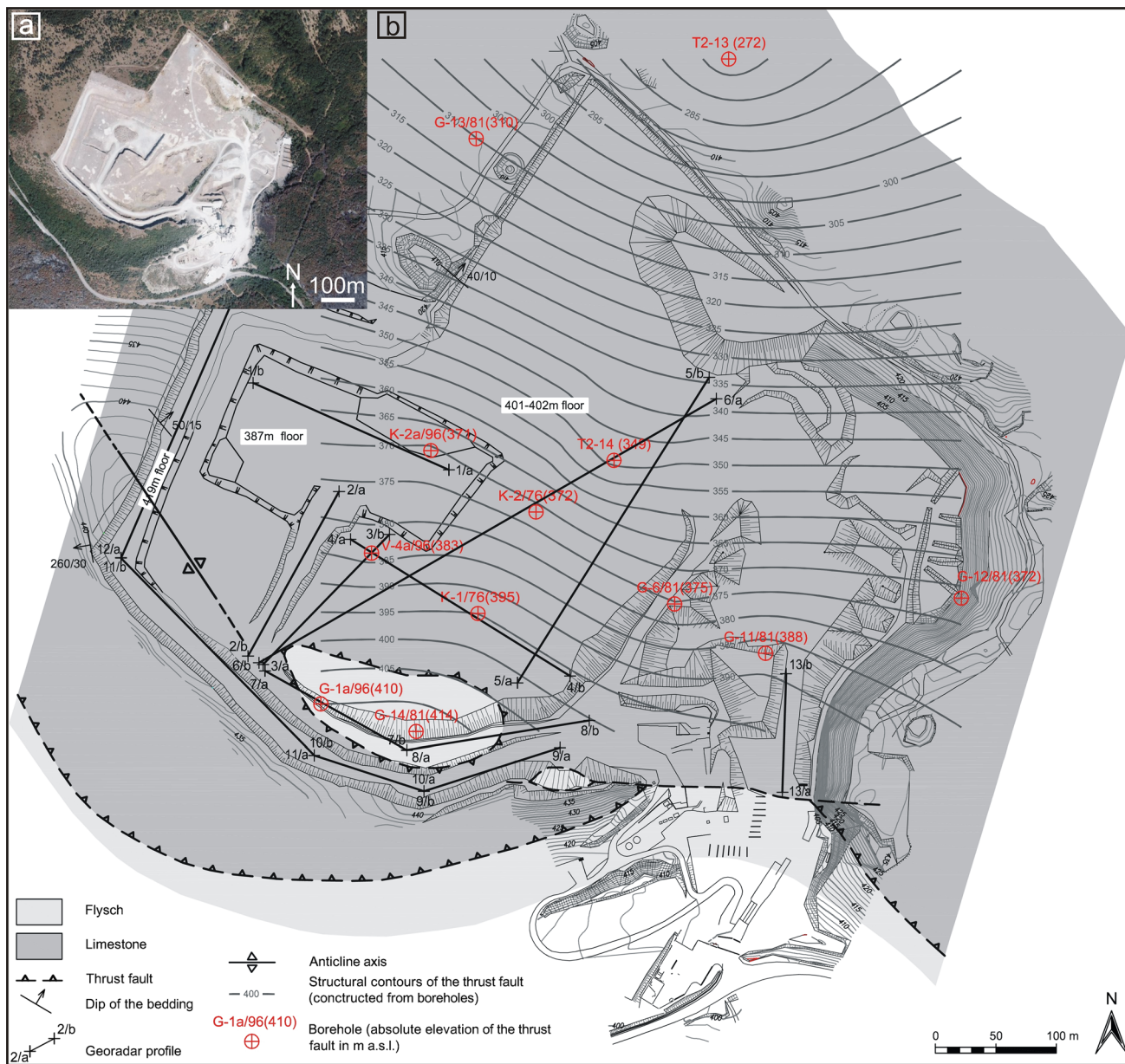
◄ **Fig. 2** **a** Orthophoto image of the Črnotiče quarry. **b** Geological map of the Črnotiče quarry with indicated boreholes (with absolute elevation of the thrust contact in m a.s.l.), structural contours of the *thrust fault*, constructed from the boreholes and GPR profiles (*a* start point; *b* end point). **c** View of the thrust contact with the hanging wall and footwall at the tectonic window in the southern part of the quarry. *Filled cavities* are also depicted. Photo was taken in the WNW–ESE direction. **d** Detail of the slightly folded thrust plane. See the person (1.8 m) for scale

method in karst environments. It has been successfully applied in various research studies, namely analysis of faults and fractures (McClymont et al. 2009; Beidinger et al. 2010; Pauselli et al. 2010), detection of karst features and cavities (Pueyo-Anchuela et al. 2009; Pavlič and Praznik 2011; dos Reis et al. 2014), determination of water table depths (Blindow et al. 2007) as well as evaluation of rock quality in quarries (Orlando 2003; Forte and Pipan 2007; Estrada-Medina et al. 2010). However, not many GPR studies have been done on thrust faults due to their complex geometry and the limited depth penetration of the GPR method.

The GPR method operates on the principles of the propagation of electromagnetic waves emitted from the transmitting antenna into the subsurface. After the signals reach an underground reflector, which can be a boundary between rock layers, a fracture or fault plane, water table, the roof of a cavity or any other feature that causes a sudden change in electromagnetic properties in the material, they are reflected back to the surface where they are detected by the receiving antenna. During this underground travelling of the signal, the time elapsed between its transmission, reflection and reception (two-way travel time) is recorded and later converted to depth (Blindow et al. 2007; Jol 2009). The depth range of the GPR depends mostly on the frequency of the antennas chosen for the survey; however, a number of other factors such as signal attenuation, presence of water and clay fractions in the ground as well as system dynamic range also have an impact on the penetration (Davis and Annan 1989; Jol 2009).

The frequency of the antennas used is, therefore, chosen on the basis of the desired penetration depth. However, this also affects the resolution of the data. Lower frequency antennas allow for greater depth ranges albeit at a reduced resolution, which makes them most suitable for structural–geological surveys where reaching greater depths is more important than achieving a high resolution. On the other hand, a GPR with high-frequency antennas reaches smaller depths but produces high-resolution data, which is, for example, a combination suitable for shallow archaeological investigations. Historical development, basic principles and applications of the GPR method have been described in various publications (Davis and Annan 1989; Daniels

1996; Annan 2002; Milsom 2003; Neal 2004; Blindow et al. 2007; Jol 2009).

Chalikakis et al. (2011) state that the GPR techniques appear to be the most popular geophysical tool for identifying and locating subsurface karst features where limestone crops out at the surface. They also note that its use becomes very limited when the surface is covered with an electrically conductive soil cover, e.g. residual clay. In karst explorations, the efficiency of the GPR on limestone formations generally increases with the use of low frequencies (under 100 MHz) and with the absence of clay soil covers, which contributes to weaker signal attenuation (Chalikakis et al. 2011). Although lower antenna frequencies increase the penetration depth, which is normally needed in karst explorations, they also decrease the resolution. Therefore, as in all GPR investigations, a compromise in the selection of the recording parameters is needed.

Data acquisition and processing

Data acquisition

The positioning of the GPR profiles in the field was carried out with defined goals and aims in mind, which were:

1. To cross the thrust contact visible in the outcrop and across the boreholes, where the exact depth of the thrust contact is known to achieve the best data correlation possible;
2. To orientate the profiles along the dip of the thrust plane to determine its characteristics with increasing GPR penetration depth and conditions at the depth limit of the GPR detection;
3. To orientate some of the profiles along the strike of the thrust-fault plane to determine its possible undulations and to link together other profiles;
4. To provide information about the true dip of the limestone strata, which can be determined either from the measurements and calculation of the apparent bedding dips, or with measurements across the known strata dip direction;
5. To detect the geometry of the prominent thrust fault-related anticline in the limestone, visible at the NW wall of the quarry;
6. To locate known and unknown filled and empty karstic voids and their relation with the host rock.

However, the present topography of the quarry surfaces, ongoing excavation works, the position of the existing boreholes and piles of dug out material that acted as obstacles for traversing the field with the GPR in straight directions also had to be taken into consideration. Thus, 13 profiles (Table 1) of various lengths and directions were

Table 1 Basic data on measured GPR profiles. Profiles shown and described in Chapter 5 are in bold

GPR profile	General direction	Length (m)	Start point elevation (m)	End point elevation (m)	Quarry floor
Profile 1	**SE–NW**	**177.0**	**387**	**387**	**1**
Profile 2	NE–SW	157.5	387	401	1–2
Profile 3	**SW–NE**	**150.0**	**401**	**401**	**2**
Profile 4	**NW–SE**	**216.8**	**401**	**401**	**2**
Profile 5	SW–NE	297.8	401	401	2
Profile 6	**NE–SW**	**436.2**	**401**	**401**	**2**
Profile 7	NW–SE	135.2	401	412	2–3
Profile 8	W–E	153.1	412	419	2–3
Profile 9	E–W	117.6	419	419	3
Profile 10	**SE–NW**	**99.6**	**419**	**419**	**3**
Profile 11	**SE–NW**	**228.4**	**419**	**419**	**3**
Profile 12	**SW–NE**	**233.3**	**419**	**419**	**3**
Profile 13	S–N	98.1	401	401	2

measured on 3 different floors and along the roads connecting the floors (Fig. 2). In the field, the positions of the existing boreholes and the starting and ending points of each profile were determined with the portable GPS receiver. The profiles were positioned either along flat working floors at different elevations of the quarry, or along inclined but smooth connecting transport roads between working floors. The topographic corrections were thus made only using the elevations of starting and ending points of the inclined profiles.

The Profile 1 was recorded at the lowermost floor (first floor, 387 m) of the quarry, while the second Profile 2 was recorded along the road from the lower to the middle floor (second floor, 401–402 m). The next four profiles (Profile 3 through Profile 6) as well as Profile 13 were located on the middle floor and the profiles (Profile 7 and Profile 8) along the road leading from the middle to the upper floor (third floor, 419 m). The rest of the profiles (Profile 9 through Profile 12) were recorded on the upper floor. All profiles except those positioned along the connecting roads to higher floors were recorded along a horizontal and even surface. On the upper floor, the profiles were oriented parallel to the quarry walls and placed in the middle of the bench with an equal distance from the wall and edge, thus minimising the effect of signal scattering (Zajc et al. 2014).

For the purpose of this study, the Mala ProEx GPR recording unit with an unshielded 50 MHz rough terrain antenna (RTA) was used. This flexible "snake-like" design of the RTA system enables easy manoeuvring through rugged terrain without affecting ground contact, therefore, shortening data acquisition time and providing good results also in difficult environment. The length of the 50 MHz

RTA is 9.25 m. The distance between the transmitting and the receiving antenna is 4 m (Mala 2009). During recording of the profiles, the time trigger mechanism with the time interval of 0.2 s was used, which requires steady movement along the profile course.

Data processing

For processing of the GPR data the Reflex-Win Version 6.0.5 from Sandmeier Software was used. First, the lengths of the profiles were calculated based on the coordinates of their start and end points. The processing steps that followed were Subtract DC Shift, Static Correction (Correct Max. Phase and Move Start time), Background Removal, Manual Gain (y) and Bandpass Frequency (low-cut 25 MHz, lower plateau 50 MHz, upper plateau 75 MHz, high-cut 150 MHz). In some cases, other processing steps were also added (Subtracting Average, Correct 3D topography).

Based on the diffractions seen in the GPR profiles in Figs. 3, 4 and 5, velocity determination was carried out by hyperbola fitting. Most diffractions within the limestone gave the signal velocity of about 120 mm/ns which corresponds to the material dielectric constant $\varepsilon = 8$. The diffractions within the flysch layers show a decrease in signal velocity to predominately 90 mm/ns, ranging between 80 and 100 mm/ns. The difference in signal velocity is the result of signals passing through a discontinuity into a material with different electromagnetic properties. In our case, the signals slow down after reaching the flysch layers. Based on Reynolds (1997) and Daniels (2004), the established parameters correspond well with the rocks in this study area.

Results

Low-frequency GPR profiling was used to study the lithological and structural characteristics of the thrust-fault contact between the limestone strata and the flysch as well as to determine the possible occurrence of cavities within the limestone and along the thrust. In this chapter, only the most representative profiles are shown and described (Profiles 1, 3 and 4 in Fig. 3, Profile 6 in Fig. 4, Profiles 10 and 11 in Fig. 5 and Profile 12 in Fig. 6); however, all the recorded profiles were used for the structural–geological reconstruction of the area (3D model in Fig. 8). The presented profiles were recorded over the outcropping limestone or cavity-filling material, and along all three floors of the quarry.

Apart from the Profile 12, all profiles show high reflectivity along a distinct discontinuity, which is the result of the different dielectric properties of the materials
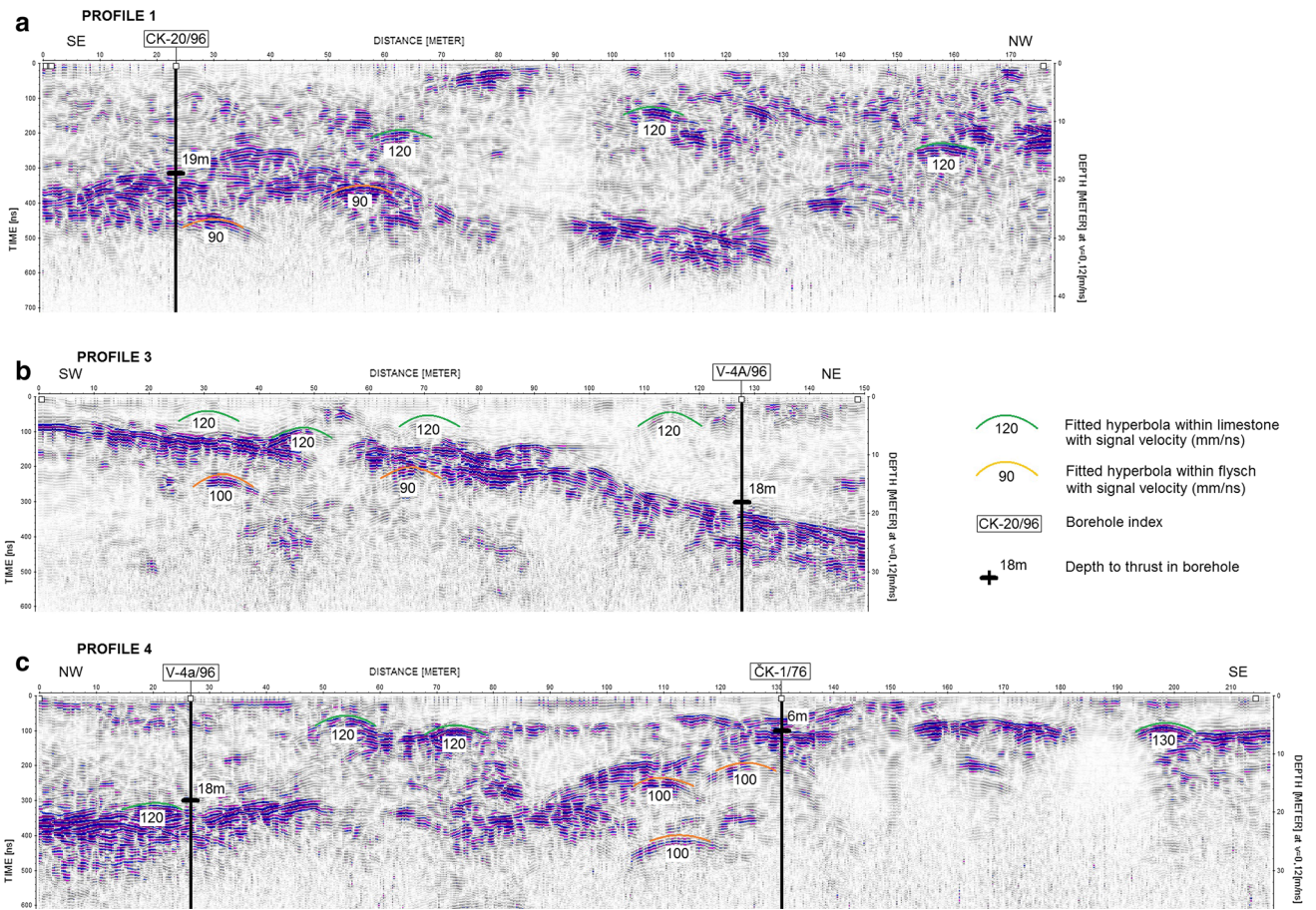
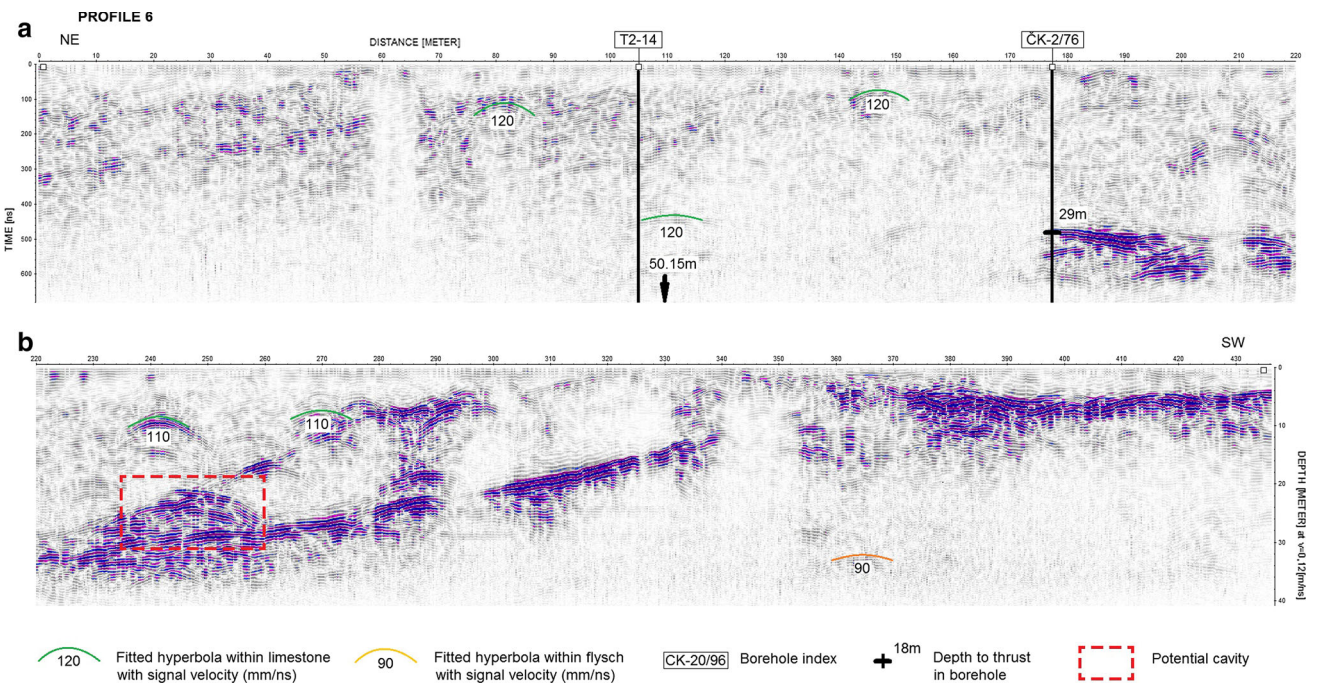Fig. 3 GPR profiles 1, 3, 4 with time and depth scale. Position in Fig. 2. a Profile 1. b Profile 3. c Profile 4

Fig. 4 GPR Profile 6 with time and depth scale. Position in Fig. 2. a 0–220 m. b 220–436 m
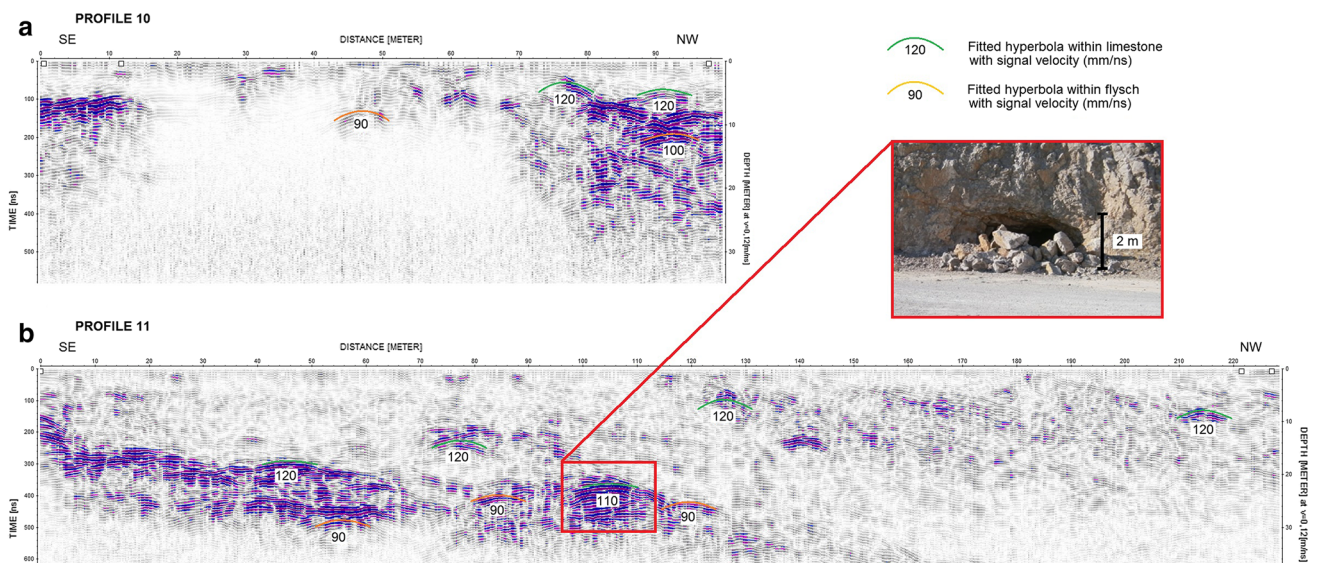
Fig. 5 GPR Profiles 10 and 11 with time and depth scale. Position in Fig. 2. **a** Profile 10. **b** Profile 11 with indicated cavity and its photo

above (limestone) and below (flysch) this reflector. The change in lithology can also be determined through signal velocity analysis. Above the reflector, the diffraction hyperbolas show the travelling velocity of about 120 mm/ns (green lines in Figs. 3, 4, 5). Below the reflector, however, signal velocity reduces to around 90 mm/ns (orange lines in Figs. 3, 4, 5). The boreholes from the quarry show that this reflector represents the thrust-fault plane between the limestone strata above and the flysch horizon below. The depth of the discontinuity derived from the GPR profiles corresponds well with the data gathered from the boreholes across which the profiles were positioned.

The Profile 1 (Fig. 3a), which is located at the lowermost floor (387 m), crosses the CK-2a/96 borehole at about 23.5 m. The depth of the thrust fault in the borehole is 19 m and corresponds well with the strong reflector seen at the same depth in the Profile 1 (Fig. 3a). Figure 3b, c shows Profiles 3 and 4, both positioned along the middle floor (401 a.s.l.), crossing the borehole V-4a/96 at 128 m (Fig. 3b) and 27 m (Fig. 3c), respectively. The Profile 4 also crosses borehole ČK-1/76 at 131 m (Fig. 3c). The depth of the thrust-fault plane determined both in boreholes and in GPR profiles is very similar. The Profile 6 (Fig. 4) was positioned across two boreholes, the T2-14 borehole at 105 m and the ČK-2/76 borehole at 177 m. Again, there is a very good correlation with the depth of the thrust-fault plane in the second borehole. The depth of the contact in the first borehole, which is 50.15 m, could not be reached with this GPR equipment as its maximum penetration in these conditions is no more than 35 m.

Other features seen in the presented profiles are the inclined continuous lines representing bedding within the limestone. These only appear in places distant enough from the thrust-fault where the layers remain relatively undamaged and the signal attenuation is not as high as when travelling through highly fractured zones. Thus, the results of the GPR profiles also provided information about the dip angles of the strata. This bedding can be seen in the Profile 4 (Fig. 3c) as the subhorizontal features starting at 60 m at the depth of about 6 m and reaching the surface at 150 m. These elements can also be clearly seen in the first 140 m of the Profile 6 (Fig. 4a), in the second part of the Profile 11 (Fig. 5a; apparent dip amounts to 13°) and throughout the whole Profile 12 (Fig. 6a). The latter was positioned far enough from the thrust to record the fairly intact anticline bedding within the limestone. The comparison of the GPR Profile 12 and the photo of the quarry wall in Fig. 6 shows that the fold geometry and limb dips in the recorded profile correspond well with the actual fold visible in the wall. The apparent dip angles of the limestone bedding in both limbs of the anticline amount to 13° in the SW limb and 16° in the NE limb. Using the apparent dip angles from the GPR results, the true dip of the SW limb was geometrically reconstructed at 264/25, which is in accordance with the dip measured in the outcrop (260/30).

By comparing the reflection pattern in the Profile 11, recorded across a known air-filled cavity seen in the quarry wall (red frame in Fig. 5a), it was also possible to determine the location of at least two other possible air-filled cavities. The first one appears in the second part of the Profile 6 between 240 and 250 m at the depth of about 21 m (red dashed frame in Fig. 4b). As this cavity is positioned directly above the thrust-fault plane, it could be
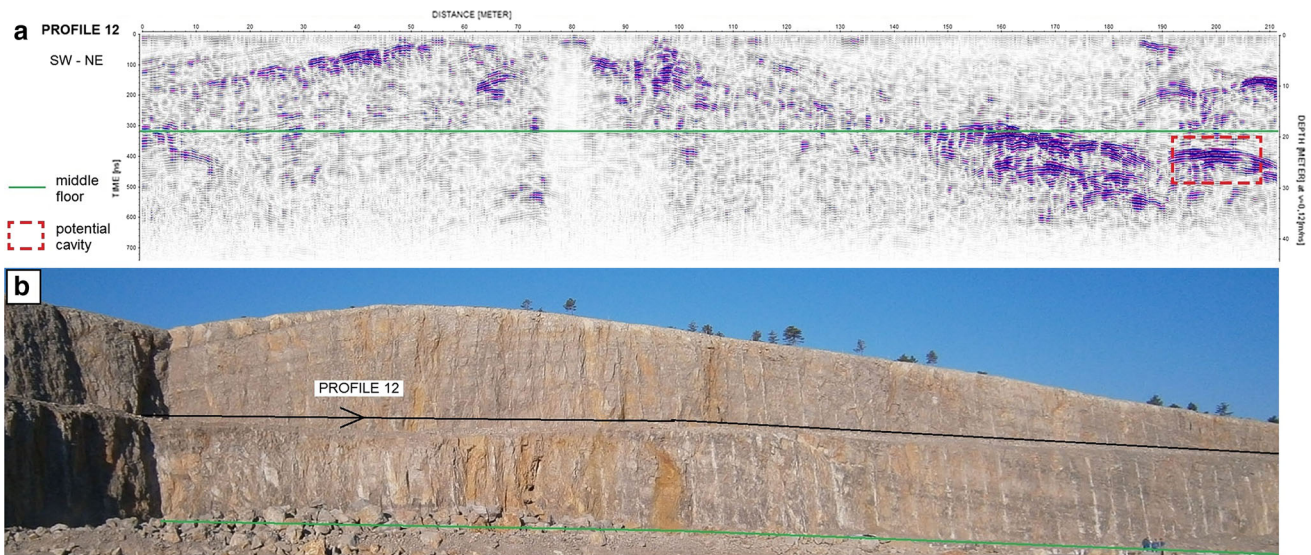
Fig. 6 a GPR Profile 12 with time and depth scale. Bedding is well pronounced, indicating *clear anticlinal shape*. There is also a potential cavity marked with the *dashed square*. b. Photo of the quarry wall with clearly visible anticline in the limestones and indicated trace of the GPR Profile 12 along the *upper floor*

the result of contact karst processes. The second cavity can be seen at the end of the Profile 12 (red dashed frame in Fig. 6a), just below the visible part of the profile. Since the area directly to the left of this cavity contains a more pronounced linear reflector, the cavity could be the result of flowing water along this solutionally enlarged bedding plane. On the other hand, there are also some narrow and spatially limited areas in the presented profiles that lack any reflections at all due to very high signal attenuation. These areas indicate the presence of cavities filled with sediments. An example of how a sediment-filled cavity is depicted in a GPR profile can be seen in Fig. 6, where the filled cavity in the top image corresponds to the absence of any signals between 76 and 82 m of the Profile 12. Other such examples also appear in the Profile 6 between 58 and 76 m (Fig. 4a), and in the Profile 10 between 16 and 44 m (Fig. 5a). In the latter, the thrust-fault plane can only be seen in the first 16 m and in the second half of the profile. In between, the fine-grained sediments that fill the cavities in the limestone above strongly attenuate the signals. These sediment-filled cavities are also clearly visible in the quarry photo in Fig. 2c.

The results give a much more precise image of the location and extension of the thrust fault throughout the quarry than the existing borehole data alone. It was possible to define the shape of the complex thrust-fault plane more accurately just by using the GPR profiles. The comparison between the structural contours of the thrust fault constructed from borehole data prior to this study and those gathered from GPR results can be seen in Fig. 7.

Discussion

The GPR profiles with the indicated thrust-fault plane and apparent dips were reconstructed in 3D to reveal the spatial extent of the thrust-fault plane and the bedding in different profiles as well as to see how well the elements of their interpretation align at the profile intersections. The interpreted thrust-fault plane, which dips in the NE direction, corresponds well with the 3D reconstruction obtained from boreholes and geological mapping. It is slightly folded and interrupted at the location of the cavities. The overall depth limit of the GPR penetration is at approximately 35 m below surface visible by the abrupt termination of the reflector that represents the thrust-fault plane. However, the signal is strongly attenuated in areas where cavities are filled with sediments. These sediments can be allochthonous, autochthonous collapse material or cave sediments (Mihevc 2000; Mihevc et al. 2002; Horaček et al. 2007). They are rich in clay and thus highly conductive. As other authors (e.g. Carriere et al. 2013) have also found, these conditions can produce clearly visible zones with poor signal strength on the GPR profiles. At the intersections of the profiles in Fig. 8, the thrust-fault plane is well aligned. The visualisation of a part of the thrust-fault plane is represented in two different directions in (Fig. 8a, b). The true

Fig. 7 Structural contours of the thrust fault, constructed from the GPR profiles. For the legend, see Fig. 2b
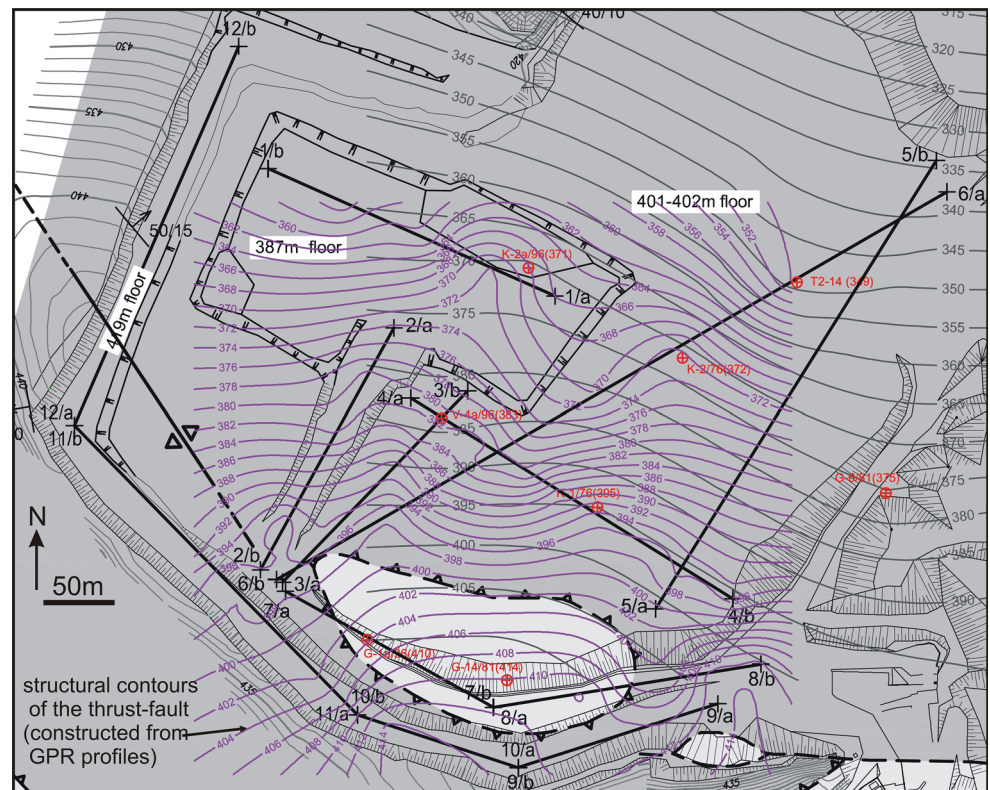
dip of the strata of the SW limb of the anticline in the SW corner of the quarry is also well presented in the 3D model, as is the anticline axis (Fig. 8b). The reconstruction of the apparent dip angles of the strata acquired from the GPR profiles gave results that correlate well with the true dip angles measured in the outcrops.

Since all GPR profiles were carefully positioned to minimise signal scattering and maximise the chances of a good correlation with the data gathered from mapping and drilling, it was possible to use all recorded profiles successfully to create a 3D model of the research area, depicting the spatial position of the Socerb thrust fault. While this model provides great insight into the subsurface and helps with the visualisation of the geometry of the thrust-fault plane, it also gives important information that is crucial for the calculations of exploitable material quantities and future excavation processes in the quarry. It will also contribute to the reduction of geological hazards due to otherwise undetected karst features during exploitation works.

Conclusions

The main objective of this study was to test the performance of the low-frequency GPR method in a structurally complex, but relatively well-known setting of the Črnotiče quarry that contains not only a thrust fault, where limestones are thrusted on flysch layers, but also karst features. The aim was to see whether the GPR results would be accurate enough to apply the method in the wider area that represents a big obstacle for the development of the new Divača–Koper railway route. The results of 13 differently oriented GPR profiles were correlated with the data collected from geological mapping and boreholes. The GPR method used gave very exact results regarding the location and spatial extend of the Socerb thrust fault when comparing the depths of the thrust in the GPR profiles with the depths derived from boreholes. The GPR results enabled the construction of a much more precise 3D shape of the trust-fault surface, then from boreholes alone. Furthermore, it was also possible to detect an air-filled cavity at the exact location as seen in the quarry face. Based on the reflection pattern produced by this cavity in the GPR profile, the locations of two other potential air-filled cavities were also determined. In addition to air-filled cavities, the GPR results also show the presence of sediment-filled cavities, which can be seen in the quarry face. The main indicator of this feature is the absence of any reflections due to very high signal attenuation. Further away from the thrust-fault zone, where the limestone strata is well preserved, apparent dip angles of
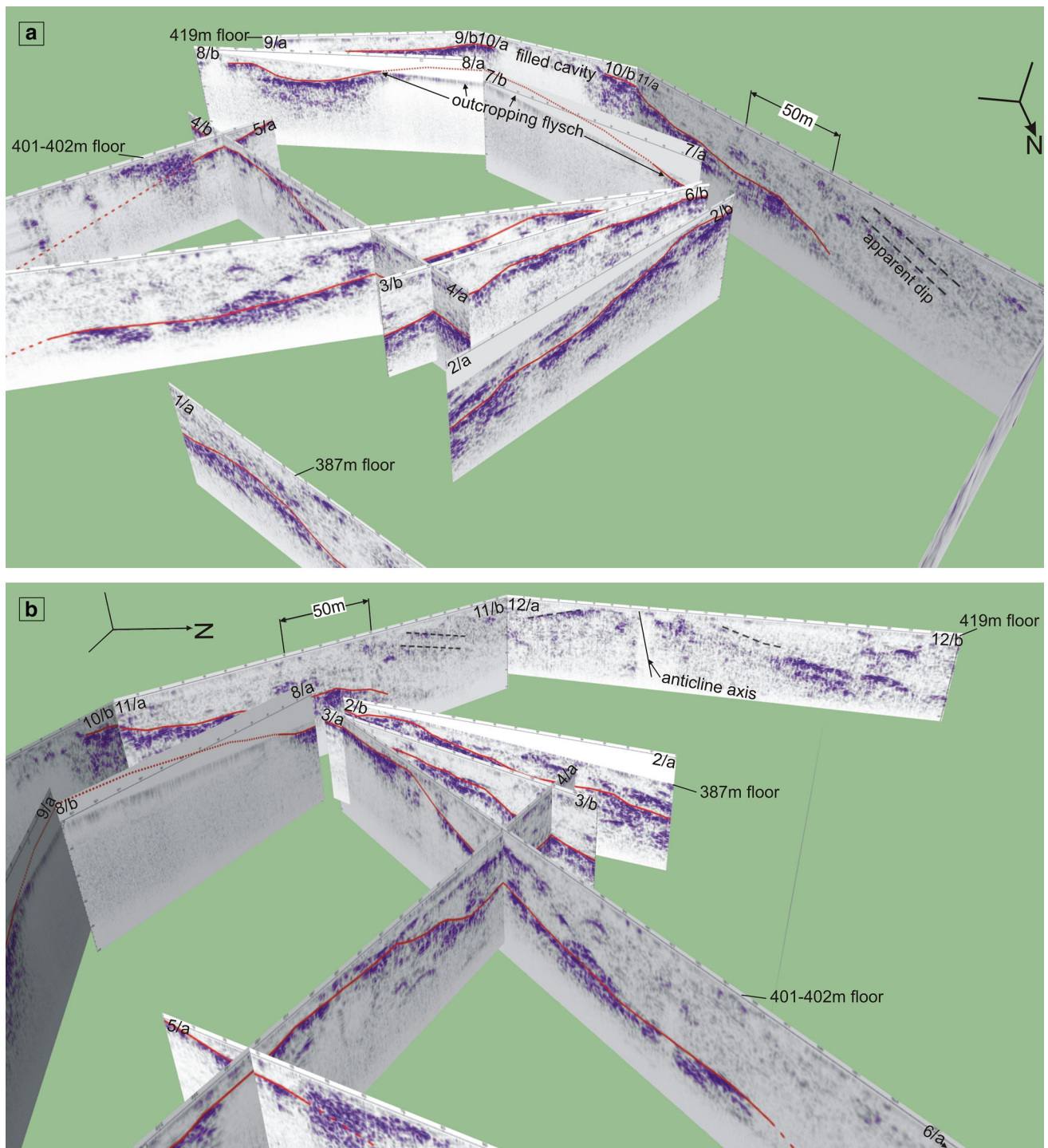
Fig. 8 3D representation of the GPR profiles with interpreted thrust-fault plane. *Continuous line* thrust-fault plane based on the GPR profiles; *dashed line*: thrust plane based on the boreholes; *dotted line* thrust-fault plane constructed above the surface based on the boreholes archive data (the area is now excavated to the present surface). **a** view in the SSE direction. **b** view in the WNW direction

the strata were also defined with GPR profiles. After their reconstruction into true dip angles and comparison with geological mapping results, they turned out to be relatively accurate.

The low-frequency GPR method has proven to be very successful in structural and karst features investigations of the Črnotiče quarry and could, therefore, be applicable in the exploration of the wider area of the Karstic thrust edge.

References

Annan AP (2002) GPR—history, trends and future developments. Subsurf Sens Technol Appl 3:253–270

Beidinger A, Decker K, Roch KH (2010) The Lassee segment of the Vienna Basin fault system as a potential source of the earthquake of Carnuntum in the fourth century A.D. Int J Earth Sci 100(6):1315–1329

Beres M, Luetscher M, Olivier R (2001) Integration of ground-penetrating radar and microgravimetric methods to map shallow caves. J Appl Geophys 46:249–262

Blindow N, Eisenburger D, Illich B, Petzold H, Richer T (2007) Ground penetrating radar. In: Knödel K, Lange G, Voigt HJ (eds) Environmental geology, handbook of field methods and case studies. Springer, Berlin, pp 283–335

Celarc B, Jurkovšek B, Placer L and Milanič B (2012) Tectonics of the region between Dinarides and Istria: Influence of plate tectonics on the infrastructure construction (2. railway track Divača–Koper) 6th Meeting of Slovenian Geotechnicians, Lipica, Slovenia, 14–15 June 2012, 49–66, SloGeD

Carriere SD, Chalikakis K, Senechal G, Danquigny C, Emblanch C (2013) Combining electrical resistivity tomography and ground penetrating radar to study geological structuring of karst unsaturated zone. J Appl Geophys 94:31–41

Chalikakis K, Plagnes V, Guerin R, Valois R, Bosch FP (2011) Contribution of geophysical methods to karst-system exploration: an overview. Hydrogeol J 19:1169–1180

Cunningham KJ (2004) Application of ground-penetrating radar, digital optical borehole images, and cores for characterization of porosity hydraulic condustivity and paleokarst in the Biscayne aquifer, southeastern Florida, USA. J Appl Geophys 44:61–76

Daniels DJ (1996) Surface Penetrating Radar, 8, 4 edn. Institute of Electrical and Electronic Engineers, London, pp 165–182

Daniels DJ (2004) Ground Penetrating Radar, 2nd edn. The Institution of Electrical Engineers, London

Davis JD, Annan AP (1989) Ground-penetrating radar for high-resolution mapping of soil and rock stratigraphy. Geophys Prospect 37(5):531–551

dos Reis JA, de Castro DL, de Jesus TES, Filho FPL (2014) Characterization of collapsed paleocave systems using GPR attributes. J Appl Geophys 103:43–56

Estrada-Medina H, Tuttl W, Graham RC, Allen MF, Jimenez-Osornio JJ (2010) Identification of underground karst features using ground-penetrating radar in Northern Yucatán, México. Vadose Zone J 9:653–661

Forte E, Pipan M (2007) GPR mass characterisation by attenuation analysis. Extended abstract. 26th Convegno Nazionale, 13–15 November 2007, Roma

Gosar A (2012) Analysis of the capabilities of low frequency ground penetrating radar for cavities detection in rough terrain conditions: the case of Divača cave, Slovenia. Acta Carsologica 41(1):77–88

Handy MR, Schmid SM, Bosquet R, Kissling E, Bernoulli D (2010) Reconciling plate-tectonic reconstructions of Alpine Tethys with the geological-geophysical record of spreading and subduction in the Alps. Earth Sci Rev 102:121–158

Horaček I, Mihevc A, Zupan Hajna N, Pruner P, Bosak P (2007) Fossil vertebrates and paleomagnetism update of one of the earlier stages of cave evolution in the classical karst, Slovenia: Pliocene of Črnotiče II site and Račiška pečina cave. Acta Carsologica 36(3):453–468

Jol HM (2009) Ground penetrating radar: theory and applications. Elsevier, Amsterdam

Jurkovšek B (2008) Geološka karta severnega dela Tržaško-komenske planote 1:25.000 (Geological map of the northern part of the Trieste-Komen plateau 1:25.000). Geological Survey of Slovenia, Ljubljana

Jurkovšek B, Toman M, Ogorelec B, Šribar L, Drobne K, Poljak M, Šribar L (1996) Formacijska geološka karta južnega dela Tržaško–Komenske planote: Kredne in paleogenske karbonatne kamnine. 1: 50.000 (Geological map of the southern part of the Trieste–Komen Plateau: Cretaceous and Paleogene carbonate rocks. 1:50.000). Geological Survey of Slovenia, Ljubljana

Korbar T (2009) Orogenic evolution of the external Dinarides in the NE Adriatic region: a model constrained by tectonostratigraphy of upper Cretaceous to Paleogene carbonates. Earth Sci Rev 96(4):296–312

Košir A (2003) Litostratigrafska revizija zgornje krede in paleogena v jugozahodni Sloveniji (Litostratigraphic revision of the upper cretaceous and the paleogene in Southwestern Slovenia). 17th Meeting of Slovenian Geologists: abstracts of papers 92–98. Department of Geology, Faculty of Natural Sciences and Engineering, University of Ljubljana

Mala (2009) ProEx—professional explorer control unit. Operating manual, Mala

McClymont AF, Villamor P, Green AG (2009) Fault displacement accumulation and slip rate variability within the Taupo Rift (New Zealand) based on trench and 3-D ground-penetrating radar data. Tectonics 28(TC4005):1–25

McMechan GA, Loucks RG, Zeng X, Mescher P (1998) Ground penetrating radar imaging of a collapsed paleocave system in the Ellenburger dolomite, central Texas. J Appl Geophys 39:1–10

Mihevc A (2000) Fosilne cevke iz brezstrope jame—verjetno najstarejši ostanki jamskega cevkarja Marifungia (Annelida: Polychaeta) (The fossilized tubes from the roofless cave—probably the oldest known remains of the cave worm Marifugia (Annelida: Polychaeta)). Acta Carsologica 29(2):261–270

Mihevc A (2007) The age of karst relief in West Slovenia. Acta Carsologica 36(1):35–44

Mihevc A, Bosák P, Pruner P, Vokal B (2002) Fosilni ostanki jamske živali Marifugia cavatica v brezstropi jami v kamnolomu Črnotiče v zahodni Sloveniji (Fossil remains of the cave animal Marifugia cavatica in the unroofed cave in the Črnotiče quarry, W Slovenia). Geologija 45(2):471–474

Milsom J (2003) Ground penetrating radar. Field geophysics, 3rd edn. Wiley, West Sussex, pp 167–178

Neal A (2004) Ground-penetrating radar and its use in sedimentology: principles, problems and progress. Earth Sci Rev 66:261–330

Orlando L (2003) Semiquantitative evaluation of massive rock quality using ground penetrating radar. J Appl Geophys 52:1–9

Otoničar B (2007) Upper Cretaceous to Paleogene forebulge unconformity associated with foreland basin evolution (Kras, Matarsko podolje and Istria; SW Slovenia and NW Croatia). Acta Carsologica 36(1):101–120

Pauselli C, Federico C, Frigeri A, Orosei R, Barchi MR, Basile G (2010) Ground penetrating radar investigations to study active faults in the Norcia Basin (central Italy). J Appl Geophys 72:39–45

Pavlič MU, Praznik B (2011) Detecting karstic zones during highway construction using ground-penetrating radar. Acta Geotechnica Slovenica 8:17–27

Placer L (2002) Predhodna objava rezultatov strukturnega profiliranja Kraškega roba in Istre, AC Kozina–Srmin, Sečovlje (Preliminary results of structural profiling of the Kras edge and Istria, Kozina–Srmin Motorway, Sečovlje). Geologija 45(1):277–280

Placer L (2005) Strukturne posebnosti severne Istre (Structural curiosity of the northern Istria). Geologija 47(2):245–251

Placer L (2007) Kraški rob. Geološki prerez vzdolž AC Kozina-Koper (Kraški rob (landscape term). Geologic section along the motorway Kozina-Koper (Capodistria)). Geologija 50(1):29–44

Placer L, Košir A, Popit T, Šmuc A, Juvan G (2004) The Buzet thrust fault in Istria and overturned megabeds in the Eocene flysch of the Dragonja Valley (Slovenia). Geologija 47(2):193–198

Placer L, Vrabec M, Celarc B (2010) The bases for understanding of the NW Dinarides and Istria Peninsula tectonics. Geologija 53(1):55–86

Pueyo-Anchuela O, Casas-Sains AM, Soriano MA, Pocovi-Juan A (2009) Mapping subsurface karst features with GPR: results and limitations. Environ Geol 58:391–399

Reynolds JM (1997) An introduction to applied and engineering geophysics. Wiley, West Sussex, p 796

Rižnar I, Koler B, Bavec M (2007) Recentna aktivnost regionalnih tektonskih struktur v zahodni Sloveniji (Recent activity of the regional geologic structures in Western Slovenia). Geologija 50(1):111–120

Sigurdsson T, Overgaard T (1998) Application of GPR for 3-D visualization of geological and structural variation in a limestone formation. J Appl Geophys 40:29–36

Vrabec M, Fodor L (2006) Late Cenozoic tectonics of Slovenia: structural styles at the Northeastern corner of the Adriatic microplate. In: Pinter N, Grenerczy G, Weber J, Stein S, Medak D (eds) The Adria microplate: GPS geodesy, tectonics and hazards, NATO science Series, IV, Earth and environmental sciences 61. Springer, Dordrecht, pp 151–168

Weber J, Vrabec M, Pavlovčič-Prešeren P, Dixon T, Jiang Y, Stopar B (2010) GPS-derived motion of the Adriatic microplate from Istria Peninsula and Po Plain sites, and geodynamic implications. Tectonophysics 483:214–222

Zajc M, Pogačnik Ž, Gosar A (2014) Ground penetrating radar and structural geological mapping investigation of karst and tectonic features in flyschoid rocks as geological hazard for exploitation. Int J Rock Mech Min Sci 67:78–87